Surfaces and Interfaces 46 (2024) 103992

Contents lists available at ScienceDirect

Surfaces and Interfaces

journal homepage: www.sciencedirect.com/journal/surfaces-and-interfaces

In situ formation of solid electrolyte interphase for improved cyclability of electrochromic tungsten oxide thin films

Shichen Weng [a,b], Chengli Zhang [c], Qiang Wang [c], Guanglong Xu [c], Jumei Zhou [b], Kunrun Song [a,b], A.A. Rogachev [d], M.A. Yarmolenko [e], Hongtao Cao [a,*], Hongliang Zhang [a,*]

[a] Laboratory of Advanced Nano Materials and Devices, Ningbo Institute of Materials Technology and Engineering, Chinese Academy of Sciences, Ningbo 315201, China
[b] Faculty of Maritime and Transportation, Ningbo University, Ningbo 315211, China
[c] Ningbo Wakan Electronic Science Technology Co. LTD, Ningbo 315475, China
[d] Optical Anisotropic Films Laboratory, Institute of Chemistry of New Materials of the National Academy of Sciences of Belarus, Minsk 220141, Belarus
[e] Francisk Skorina Gomel State University, 104, Sovetskaya Street, Gomel 246019, Belarus

ARTICLE INFO

Keywords:
Electrochromism
Tungsten oxide
Solid electrolyte interphase
Atomic layer deposition

ABSTRACT

Tungsten oxide (WO_3) is highly regarded as one of the most promising working electrodes for electrochromic devices due to its large optical modulation, however, it suffers from degradation at the WO_3/electrolyte interface. Herein, we developed an ALD-Al_2O_3/Li-based electrolyte hybrid layer as organic/inorganic solid electrolyte interphase (SEI) to improve the cyclic stability of the WO_3 thin films. *In situ* formation of SEI has been confirmed by an analysis of components (such as Li_2CO_3, Li_2O, and PC) of the electrochromic WO_3 thin films with the ALD-Al_2O_3 interface layer after electrochemically cyclic treatment. As for comparative analysis of microstructural and electrochemical properties of the electrochromic WO_3 thin films with and without the ALD-Al_2O_3 interface layer, we emphasize that the SEI, introduced by the ALD-Al_2O_3 interface layer and produced by electrochemical cycling, embodies its optimality properties. With the introduction of SEI, the cyclic stability of the WO_3 thin film can be significantly enhanced, allowing for a stable transmittance modulation (1500 cycles with 94 % retention). This work offers a new strategy to improve the cyclic stability of WO_3 thin films and enlightens the design on stable interface for electrochromic electrodes.

1. Introduction

Electrochromic devices (ECDs) are of interest because of their low power consumption and high transmittance contrast. ECDs have been extensively investigated for many potential applications such as skylights, rear-view mirrors, and electrochromic smart windows for buildings [1–4]. Typical ECDs consist of five layers: an electrochromic (EC) layer, an ion-conducting layer, an ion-storage layer, and transparent electrodes on both sides [5,6]. EC layer materials can be divided into cathodic and anodic coloration materials. Among cathodic electrochromic materials, tungsten oxide (WO_3) is considered one of the most promising candidates for commercialization owing to its large transmittance modulation and high coloration efficiency. Presently, the lithium perchlorate ($LiClO_4$)-propylene carbonate ($C_4H_6O_3$, PC) electrolyte is the most commonly used liquid electrolyte for WO_3-based ECDs [7,8]. However, during the electrochemical cycling process, undesired side reactions between WO_3 electrode and electrolyte continuously occur, with the accumulation of the interfacial degradation, resulting in decreased cyclic stability and rate capability [9–11]. In fact, the development of the WO_3 EC layer with long-term cyclic stability has become a challenge that must be surmounted for the commercial viability of WO_3-based ECDs.

Actually, intensive previous investigations have been dedicated to improving the properties of the EC layer, such as depositing a silicon nitride (Si_3N_4) thin film onto the WO_3 thin film by pulsed DC reactive magnetron sputtering [12]. The Si_3N_4 film is used as the electron-blocking layer to reduce the leakage current of the EC, and the Si_3N_4 thin film can prevent contact between WO_3 and water, thereby improving the cycling durability. The interface between EC materials and electrolytes has been shown to be crucial in determining the electrochemical and EC properties [13]. Very recently, the strategy of adding a protective layer (such as Ta_2O_3 [14], SnO_2 [15], Nafion-film [16]) onto the electrochromic film has emerged as a viable solution. Unfortunately, the underlying variations of the protective layer during cycling

* Corresponding authors.
E-mail addresses: h_cao@nimte.ac.cn (H. Cao), zhanghl@nimte.ac.cn (H. Zhang).

https://doi.org/10.1016/j.surfin.2024.103992
Received 23 October 2023; Received in revised form 24 January 2024; Accepted 26 January 2024
Available online 1 February 2024

have not been entirely understood yet, only as a means of interface modification largely unexplored. Remarkably, in the field of Li-ion batteries (LIBs), extensive research has already been conducted on electrode protective layers, known as the artificial solid electrolyte interphase (SEI) layer.

SEI layers are considered the most crucial yet least understood phenomena in batteries. SEI is generated to fully passivate the electrode/electrolyte interface after the irreversible decomposition of unstable ingredients, including solvents, anions, and additives upon initial charging and discharging processes of LIBs, this passivation layer exhibits characteristics of a solid electrolyte and acts as an electronic insulator while serving as an excellent conductor for Li-ions [17,18]. An ideal interface is expected to meet several requirements, including chemical/electrochemical stability with electronic insularity, mechanical robustness and stable ion pathways [19]. In light of the flaws of the natural interface, which is the interface *in situ* formed by solvent decomposition, researchers have pursued various strategies to obtain ideal interfaces with targeted properties, such as optimizing the electrolyte formulation and designing artificial protective films. Empirical evidence demonstrates that a ~9-Å-thick Al_2O_3 interface layer deposited by atomic layer deposition (ALD) effectively inhibits the formation of the unstable interface and survives the rigors of electrochemical cycling for at least 100 cycles, significantly improving the cycling stability of the MnO electrode [20]. Introducing ALD oxide interface layer as artificial SEI on Li-ion battery electrodes has become popular because of its unique advantages in high conformality and controllable thickness at the angstrom level. For instance, a ~2-nm-thick ALD-Al_2O_3 layer could prevent side reactions during electrochemical and stabilize the structure of the silicon column, the silicon electrode with the ALD-Al_2O_3 layer shows high coulombic efficiency and good cycling performance [21]. The attachment of the MoO_3 particles to the conductive additives is improved by using the ALD-Al_2O_3 layer which reduces the detachment of particles during the volume changes [22,23]. However, with regards to electrochromism, to the best of our knowledge, no research has been conducted on the interfacial modification of WO_3 thin film by ALD-Al_2O_3 interface layer, and the understanding of the Al_2O_3-involved SEI formation is very limited.

In this work, an ALD-Al_2O_3/Li-based electrolyte hybrid layer as organic/inorganic SEI is proposed to improve the cyclic stability of the WO_3 thin films, as shown in schematic Diagram 1. The SEI has been demonstrated to be very effective in improving the stability of the electrochromism by comparative analysis of microstructural and electrochemical properties of the electrochromic WO_3 thin films with and without the ALD-Al_2O_3 interface.

2. Experimental

2.1. Preparation of thin films

The WO_3 thin films were deposited on the ITO-coated glass at a substrate temperature of 200 °C by electron beam evaporation technique (MUE-ECO made in ULVAC, Japan). The deposition processes occurred in the vacuum of 4×10^{-3} Pa, Several pure WO_3 particles with the diameter of ~ 3 mm in a tungsten crucible were bombarded by an electron beam of 10 kV. The deposition rate and thickness of the film were controlled by a quartz-crystal film-thickness monitor at 0.15 nm/s and 300 nm, respectively.

ALD coating of Al_2O_3 was performed in a commercial thermal type ALD reactor equipment (TALD-150D, Kemicro) with 6-inch reaction chamber. Trimethylaluminum (TMA) and H_2O were used as reaction precursors. TMA with purity of 99.9 % made by AimouYuan (Nanjing, China) and H_2O were evaporated at 150 °C. N_2 (7 sccm) was served as both the carrier and purging gas for the precursor vapor. The deposition was directly conducted on the as fabricated WO_3/ITO-coated glass, the glasses were placed in the center of the cavity and maintained at 150 °C during the deposition process. 0.025 s and 0.015 s pulses were used for TMA and H_2O precursors with a 20 s N_2 purge between precursors. Using 10 cycles of ALD Al_2O_3, the deposited Al_2O_3 thickness is estimated to be approximately 1 nm, as determined by ellipsometry. The WO_3 thin film with ALD-Al_2O_3 thickness of 1 nm was selected as the optimized one, since it showed better electrical, electrochemical, and electrochromic performance, the results and discussion are described in the supplementary information S1.

2.2. Characterization

The structure of the WO_3 thin films was analyzed by X-ray diffraction (XRD, Bruker D8 Advance with Cu Kα radiation (λ=0.154178 nm) and a theta-2theta configuration). The surface chemistry of the WO_3 thin film was performed by X-ray photoelectron spectra (XPS, Axis Ultra DLD), using Al Kα (1486.6 eV) radiation as an X-ray source with a voltage of 15 kV and a power of 120 W at a pressure of $\sim 5 \times 10^{-9}$ Torr. The XPS core level spectra were fitted using the Liner and Shirley type background. The microstructures and elemental analysis of the WO_3 films with the ALD-Al_2O_3 layer were examined by high-resolution transmission electron microscopy (HRTEM, Tecnai F20, FEI) and scanning electron microscope (SEM, Verios G4 UC, Thermo Scientific). *In situ* transmittance spectra were achieved via visible spectroscopy (723 PC, Jinghua, Shanghai) and electrochemical workstation (CHI660D, Chenhua, Shanghai) with a traditional three-electrode cell. A platinum sheet and KCl saturated Hg/$HgCl_2$ were used as counter electrode and reference electrode, respectively. The galvanostatic charge-discharge (GCD) and cyclic voltammetry (CV) measurements were carried out by applying a corresponding current or voltage. The electrochemical impedance spectra (EIS) were measured on an electrochemical workstation (IM6, Zennium) in the frequency range from 100 mHz to 100 kHz.

3. Results and discussion

3.1. Electrochromic performance of the thin films

Fig. 1a and b depicts the *in situ* visible transmittance spectra (at λ_{633nm}) of the WO_3 thin films with and without the ALD-Al_2O_3 interface layer under −1.0/1.0 V voltage for 35 s/40 s, respectively. The maximum transmittance modulation (ΔT) of the WO_3 thin film without the ALD-Al_2O_3 interface layer is measured to be 90 % at the first cycle. Fig. 2a reveals a gradual decrease in the optical modulation (ΔT≈70 %, 75,000 s, 1000th cycle) with increasing cycle number for the WO_3 thin film without the ALD-Al_2O_3 interface layer, ultimately leading to a failure of electrochromic performance after 1464 cycles (112105s). In contrast, the cyclic stability of transmittance modulation (>80 %) of the WO_3 thin film with the ALD-Al_2O_3 interface layer is expected to remain steady after 1500 cycles (112500s), as shown in Fig. 1b. The ΔT of the WO_3 thin film with the ALD-Al_2O_3 interface layer drops from 85 % for the first cycle to > 80 % for the 1500th cycle. A comprehensive comparison of the cycle number, the running time, and the amount of retention after cycling between the WO_3 thin film with the ALD-Al_2O_3 interface layer and other reported works are presented in Table S2. The obvious superiorities of this work are demonstrated with 94 % transmittance modulation retention after 1500 cycles and 104 % current density retention after 3000 cycles (Fig. S5). Moreover, Fig. S6 shows that the optical modulation of the WO_3 thin film with the ALD-Al_2O_3 interface layer is well-maintained, with a ΔT of more than 70 % even after the 3000th cycle (225000s). Besides, there is some evidence to suggest that the ΔT of the WO_3 thin film without the ALD-Al_2O_3 interface layer is higher than that of the WO_3 thin film with the ALD-Al_2O_3 interface layer at the first cycle in the *ex situ* transmittance spectra (Fig. S7). This distinction is further exemplified in studies using the coloring/bleaching response times (the time required to achieve a 90 % change in transmittance between the colored and bleached states [24]).

Fig. 1c and f show the coloring/bleaching time of the WO_3 thin film without and with the ALD-Al_2O_3 layer at the first electrochemical cycle.

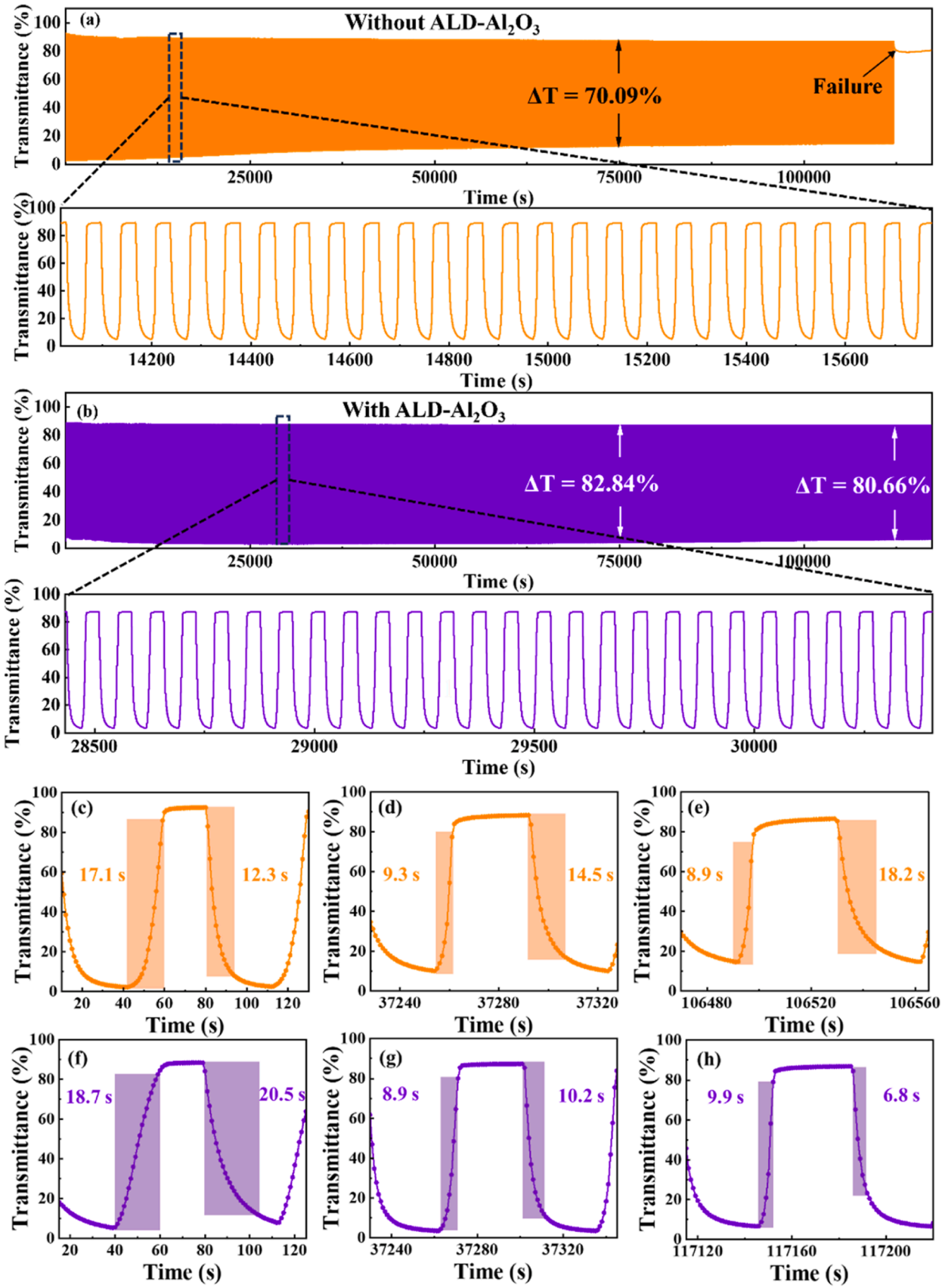

Fig. 1. *In situ* visible transmittance spectra at $\lambda_{633\ nm}$ of the WO_3 thin film (a) without and (b) with the ALD-Al_2O_3 interface layer. The coloring/bleaching response times of the WO_3 thin film (c–e) without and with (f–h) the ALD-Al_2O_3 interface layer.

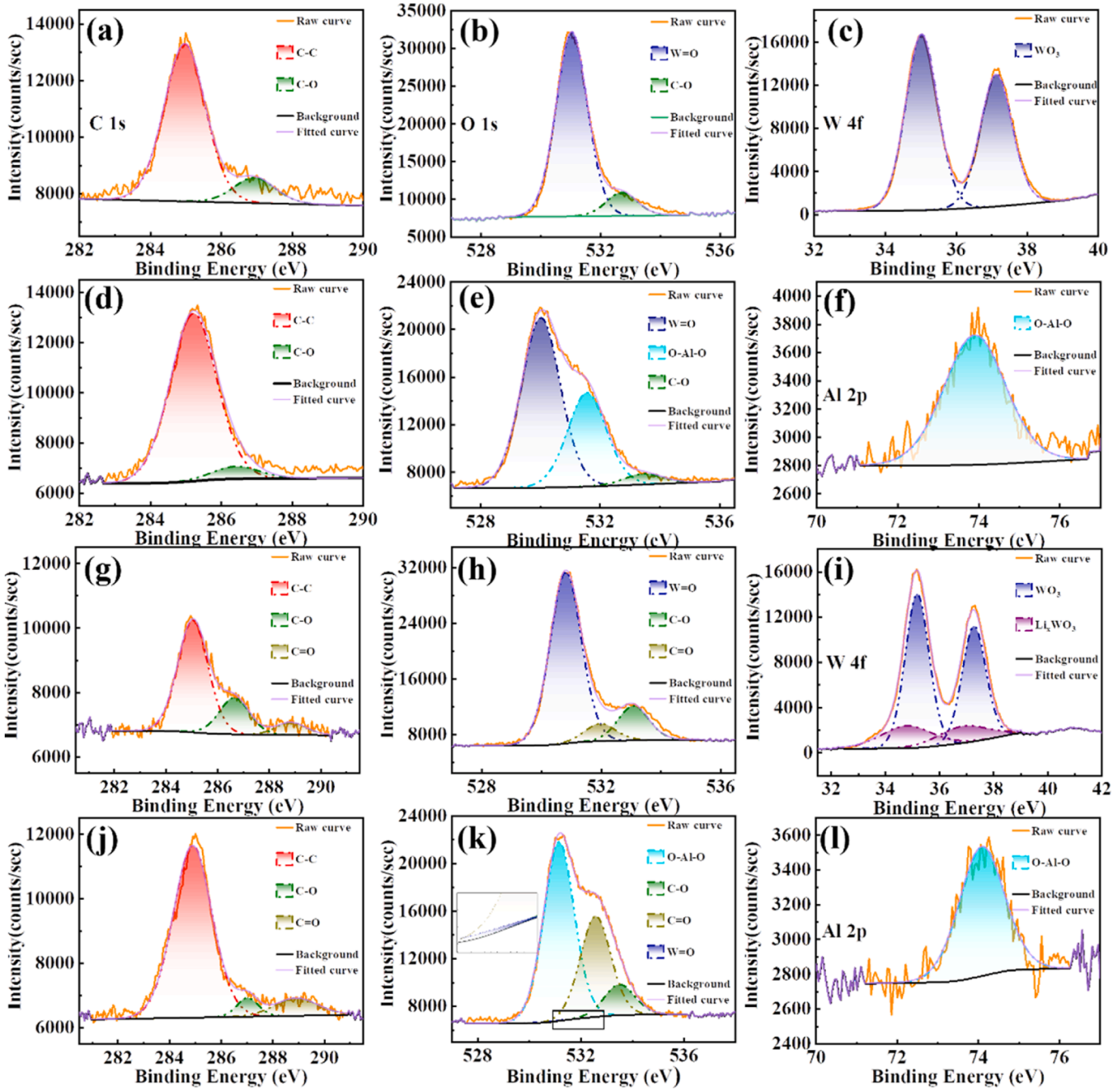

Fig. 2. XPS spectra of the as-deposited WO_3 thin film (a–c) without and (d–f) with the ALD-Al_2O_3 interface layer. XPS spectra of the WO_3 thin film (g–i) without and with (j–l) the ALD-Al_2O_3 interface layer after 50 electrochemical cycles.

The WO_3 thin film with the ALD-Al_2O_3 interface layer shows longer response times (20.5 s/18.7 s) than the WO_3 thin film without the ALD-Al_2O_3 interface layer (12.3 s/17.1 s). This can be attributed to the pinehole-free ALD-Al_2O_3 layer blocking the diffusion of lithium ions and the penetration during the initial cycling process, consistent with that in the previous report [25]. What is interesting in Fig. 1g and 1h is rapid decrease of the WO_3 thin film with the ALD-Al_2O_3 interface layer in the response times as the number of cycles increases. This can be explained by the transformation of the Al_2O_3 layer into Li-Al-O during cycling. Li-Al-O is an ionic conductor that facilitates the transport of Li ions [22, 23]. As shown in Fig. 1d and 1e, the coloring/bleaching time of the WO_3 thin film without the ALD-Al_2O_3 layer is changed from 14.5 s/9.3 s to 18.2 s/ 8.9 s, indicating a degradation of its rate performance. Conversely, the response times of the WO_3 thin film with the ALD-Al_2O_3 interface layer tend to be more stable and faster. It seems possible that the remarkably optical improvement of cyclic stability can be attributed to improved cyclability of the interface between electrochromic tungsten oxide electrodes and the electrolyte.

3.2. *XPS of the thin films*

The XPS results of the WO_3 thin films without and with the ALD-Al_2O_3 interface layer in the as-deposited state and after 50 electrochemical cycles are shown in Fig. 2. The C 1 s spectra of the WO_3 thin films without and with the ALD-Al_2O_3 interface layer after cycling has been partitioned a peak at 288.8 eV characteristic of the C = O present in CO_3, which is attributed to Li_2CO_3, and lithium alkyl carbonates produced during cycling [10,26]. In addition, the C 1 s spectra can be fitted

into two peaks characteristic of C—C (285 eV) and C—O (286.9 eV), as shown in Fig. 2a, d, g, and j. The O 1 s spectra of the as-deposited thin films are shown in Fig. 2b and e. A peak centered at 531.5 eV is observed for the WO_3 thin film with the ALD-Al_2O_3 interface layer, matching the Al 2p spectra for the as-deposited WO_3 film with Al_2O_3 interface layer (Fig. 2f). As the WO_3 thin films without and with the ALD-Al_2O_3 interface layer is cycled with 50 electrochemical cycles, the C—O and C = O peaks appear, and the $W = O$ peak is barely visible for the WO_3 thin film with ALD-Al_2O_3 interface layer, as shown in Fig. 2h and k. Table 1 presents the O 1 s XPS results of the WO_3 thin films without and with the ALD-Al_2O_3 interface layer in the as-deposited state and after 50 electrochemical cycles. The peak area of $W = O$ in the XPS spectra of the WO_3 thin film with the ALD-Al_2O_3 interface layer is almost negligible (0.57 %) after cycling. The increase (74.9 %) in the $W = O$ peak area of XPS spectra accounts of the WO_3 thin film from without to with the ALD-Al_2O_3 interface layer after cycling suggests the effectiveness of the Al_2O_3 interface layer in alleviating the interfacial degeneration by the potential irreversible reaction between electrolyte and WO_3 electrode. Moreover, the C = O peak area in the XPS spectra of the WO_3 thin film with the ALD-Al_2O_3 interface layer is notably higher than that of the WO_3 thin film without the ALD-Al_2O_3 interface layer after cycling. This observation may be attributed to the space for side-reaction products formation is constrained by the surrounding ALD-Al_2O_3 coating, allowing for quicker interface densification and *in situ* formation of organic/inorganic hybrid solid electrolyte interphase on the WO_3 thin film during the electrochemical cycling. The Al_2O_3-induced SEI preventing the electron transfer process, thereby reducing the reduction reaction of the electrolyte and increasing the organic component of the SEI layer [20,27]. Fig. 2c shows the W 4f XPS spectra of the as-deposited WO_3 thin films with Al_2O_3 interface layer that contain two peaks correspond to W $4f_{7/2}$ and W $4f_{5/2}$ spin-orbit split peaks, respectively [28]. The spectra of the cycled samples are fitted into four peaks, indicating the presence of W^{6+} (bleached) and W^{5+} (colored) valence states (Fig. 2i) after cycling [29,30].

3.3. TEM of the thin films

The microstructures of the WO_3 thin film with the ALD-Al_2O_3 interface layer after electrochemical cycling are further analyzed by high-resolution transmission electron microscopy (HRTEM), as shown in Fig. 3. The energy-dispersive X-ray spectroscopy (EDX) mapping displays that Al and O signals uniformly appear on the surface, originating from the fully conform and uniform ALD-Al_2O_3 layer on the WO_3 electrode (the corresponding ADF-STEM image of the EDX mapping images are shown in Fig. S8a). A pronounced boundary without a lattice fringe is observed for the WO_3 thin film with the ALD-Al_2O_3 interface layer in Fig. 3b. This indicates that the Al_2O_3 layer and WO_3 thin film have an amorphous nature, consistent with the above XRD results (Fig. S8b). The selected area electron diffraction (SAED) pattern (inset) shows lattice spacings of 0.24 nm, 0.135 nm, and 0.12 nm, which is assigned to the (−311), (132), and (−424) planes of Li_2CO_3, respectively. To further investigate the structure of the solid electrolyte interphase (SEI), the Digital Micrograph (DM)-based inverse Fast Fourier Transform (FFT) is employed on regions 1–4 of Fig. 3c, as depicted in Fig. 3d–g. There is a lattice fringe with a spacing of 0.25 nm and a pair of bright spots related to the (212) faces of LiCl in Fig. 3d. Furthermore, lattice fringes with spacings of 0.27 nm and 0.21 nm are observed in Fig. 3e and f, corresponding to the (101) face of LiOH and the (−221) face of Li_2O, respectively [31–36]. These inorganic species are typically regarded as effective components of the SEI layer that can be formed on the electrode during cycling. Such species can be produced as by-products of the electrolyte solution (PC-$LiClO_4$) and contribute to the overall stability and passivation of the SEI layer. A number of lattice fringes similar to those of PC are observed in thin film (Fig. 3g). These substances could be the products of side reactions involving PC molecules during cycling and the chelates formed by the complexation of PC molecules with Li ions [11]. It is well known that typical organic components of the SEI layer produced during electrochemical cycling of PC-based electrolyte solutions include $(CH_2OCO_2Li)_2$, $ROCO_2Li$, ROLi, and others, are abundantly present on the surface of the thin film. The TEM results indicate that the microstructures of the WO_3 thin film with the ALD-Al_2O_3 interface layer conform to the compact-stratified layer (CSL) model after cycling. According to this classic SEI mode, the inner layer of SEI in contact with the electrode predominantly comprises inorganic materials (such as Al_2O_3), while the outer layer in contact with the electrolyte primarily consists of organic and other inorganic components [37,38]. These observations demonstrate that a stable and ultra-thin organic-inorganic hybrid SEI layer is formed on the WO_3 thin film with the ALD-Al_2O_3 interface layer.

Table 1
The O 1 s XPS results of the as-deposited and cycled WO_3 thin films without and with the ALD-Al_2O_3 interface layer.

Contributions	Samples			
	WO_3 (as-deposited)	WO_3/Al_2O_3 (as-deposited)	WO_3 (after 50 cycles CV)	WO_3/Al_2O_3 (after 50 cycles CV)
O-Al-O	0	33.37 %	0	57.35 %
C—O	11.56 %	7.42 %	13.78 %	9.84 %
C = O	0	0	11.32 %	32.24 %
$W = O$	88.44 %	59.21 %	74.9 %	0.57 %
Total	100 %	100 %	100 %	100 %

3.4. SEM of the thin films

The interfacial degradation at the WO_3/electrolyte interface can be attributed to two fundamental reasons. (i) The sustained side reaction leads to the formation of a thick interface. (ii) The cracks produced during cycling can expose the fresh WO_3 surface, initialing the formation of a new interface. To gain an understanding of the interfacial degradation, TEM and SEM techniques are conducted. Fig. S9 shows the TEM images of the WO_3 thin film without the ALD-Al_2O_3 layer after 10 electrochemical cycles, revealing the presence of a ~10 nm-thick interface on the WO_3 surface. SEM micrographs in Fig. 4 provide a closer look at the surface and cross sections for the WO_3 thin films without and with the ALD-Al_2O_3 interface layer after 50 electrochemical cycles. It is observed that the thickness of the interface for the bare WO_3 increases to 80 nm after 50 cycles (Fig. 4a and 4b). It is reported that the PC-based electrolyte has a high reduction potential (~0.7 V), and is prone to react on the electrode surface [10]. The sacrificial decomposition of the PC electrolyte results in the formation of lithium alkylcarbonates and Li_2CO_3. The interface of the WO_3 thin film without the ALD-Al_2O_3 is expected to consist of WO_3, PC, lithium alkylcarbonates, and Li_2CO_3. Unfortunately, this *in situ* formed interface has poor electron-insulating capability, which fails to effectively isolate the electron tunneling from the highly negatively charged electrode to the electrolyte components. As a result, the PC electrolyte continuously decomposes during cycling, resulting in the formation of a thick interface.

Additionally, the *in situ* formed interface is not strong enough to endure the mechanical deformation of the WO_3 thin film during the ion intercalation, resulting the cracks on the surface (Fig. 4c) [10,18,20]. These cracks allow the infiltration of electrolyte into the film and break the interface, exposing the fresh WO_3 surface. This lead to the formation of a new interface, as shown in Fig. S10. As the number of cycles increases, the WO_3 thin film without the ALD-Al_2O_3 layer gets consumed, eventually leading to the failure of the electrochromic performance.

On the other hand, the WO_3 thin film with the ALD-Al_2O_3 interface layer shows no additional layer (Fig. 4d and 4e) on its surface after electrochemical cycling. The surface remains relatively intact, as shown in Fig. 4f. The presence of the ALD-Al_2O_3 layer effectively constrains the space for side-reaction products formation, facilitating quicker interface

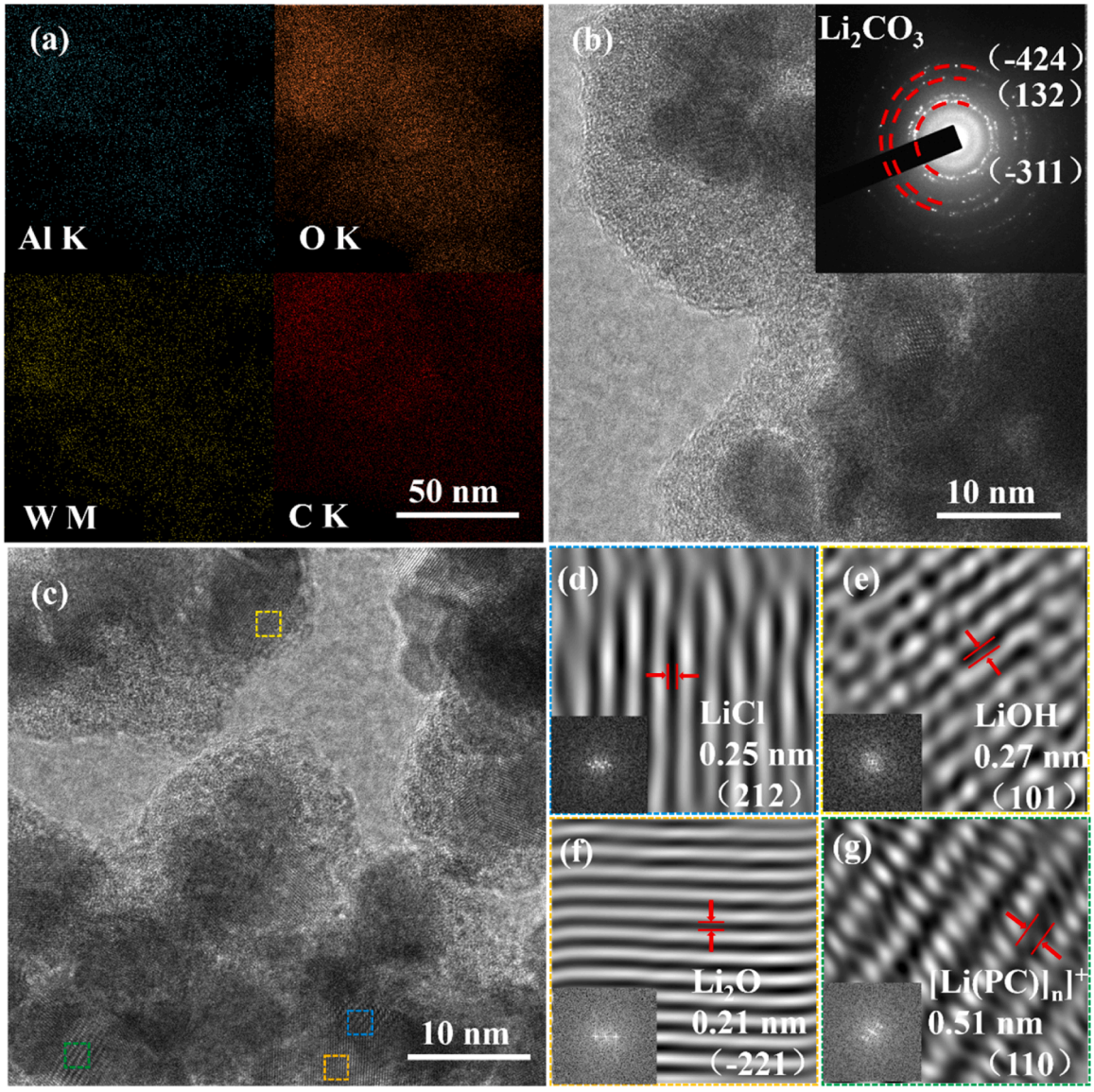

Fig. 3. (a) The energy-dispersive X-ray spectroscopy (EDX) mapping of the WO_3 thin film with the ALD-Al_2O_3 interface layer. (b) The TEM image and selected area electron diffraction (SAED) pattern (inset) of the WO_3 thin film with the ALD-Al_2O_3 interface layer. (c) The high-resolution TEM (HRTEM) image of the WO_3 thin film with the ALD-Al_2O_3 interface layer, marked by dotted circle. (d–g) The inverse Fast Fourier Transform (FFT) filtered HRTEM images and FTT patterns (inset) of the characteristic region of the WO_3 thin film with the ALD-Al_2O_3 interface layer.

densification [25]. The interface involving Al_2O_3 hinders the sustained decomposition of the electrolyte. Furthermore, the completely conformal coating of ALD-Al_2O_3 reduces the occurrence of small cracks and pinholes, which are the main causes of extensive cracking [22]. This reduction in cracking allows the WO_3 thin film to avoid the generation of a new surface during cycling. Overall, these results demonstrate that the ALD-Al_2O_3 interface layer acts as a protective barrier, preventing the sustained reaction of the electrolyte and reducing cracks on the surface of the WO_3 thin film. This depresses the continuous thickening and degradation of the interface.

3.5. Electrochemical performance of the thin films

The cyclic voltammetry (CV) test is employed to evaluate the ions detercalation/intercalation processes of the WO_3 thin films with and without the ALD-Al_2O_3 layer. As shown in Fig. 5a, the peak values of the CV curves are increased accordingly with the scan rate with the applied potential between −1.0 and +1.0 V. The result shows that the WO_3 thin film with the ALD-Al_2O_3 interface layer exhibits normal redox behavior.

In general terms, the switching speed of electrochromic thin film mainly depends on the ion-diffusion coefficient and ion diffusion distance [39]. The Li-ion diffusion coefficient (D) can be calculated using the following equation:

$$I_p = 2.72 \times 10^5 \times n^{3/2} \times A \times D^{1/2} \times C_0 \times v^{1/2}$$

where I_p is the peak current of the CV curve, n, A, C_0, and v refers to the number of electrons participating in the reactions, the contact area between the thin film and electrolyte, the Li ions concentration in the electrolyte, and the scan rate, respectively [40]. As illustrated in Fig. 5b, the diffusion coefficient (D) is respective to be 2.799×10^{-10} cm^2 s^{-1} and 1.132×10^{-10} cm^2 s^{-1} for the WO_3 thin films without and with Al_2O_3 interface layer. Notably, the diffusion coefficient of the WO_3 thin film with the ALD-Al_2O_3 interface layer is slightly lower than that of the WO_3 thin film without the ALD-Al_2O_3 interface layer, consistent with the longer response times that the WO_3 thin film with the ALD-Al_2O_3 interface layer exhibits at the beginning of the electrochemical cycling. These results demonstrate that the ALD-Al_2O_3 interface layer can act as a

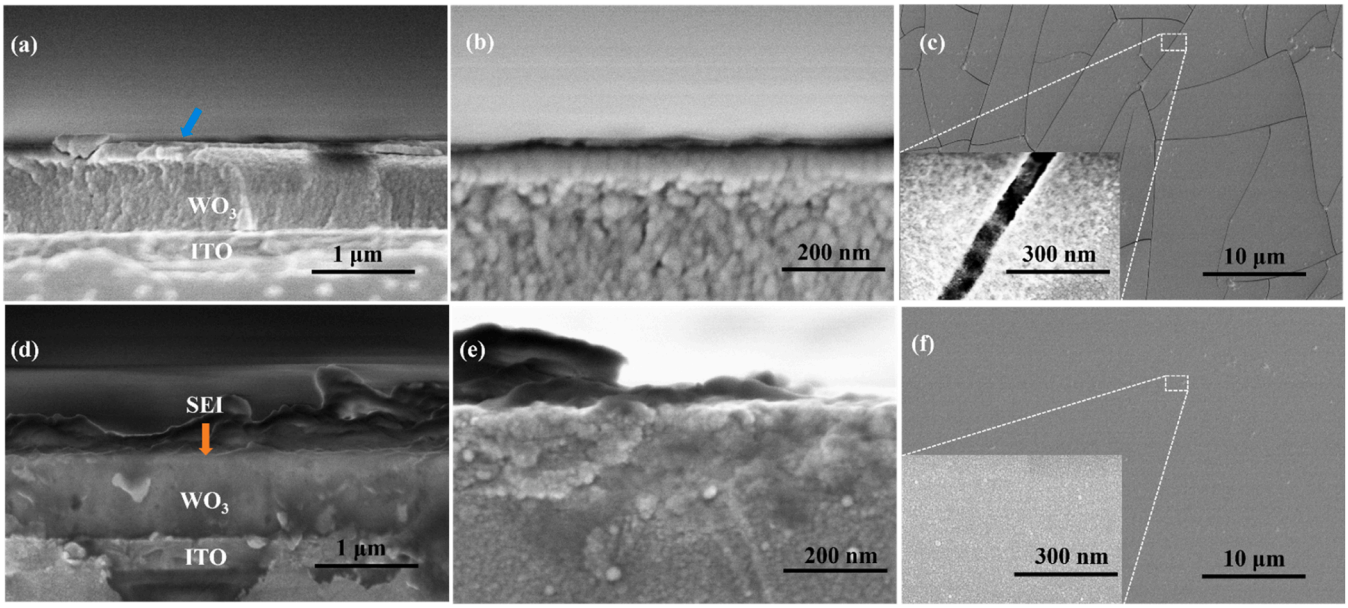

Fig. 4. The SEM micrographs of the top surface and cross sections for cycled WO_3 thin films (a–c) without and (d–f) with the ALD-Al_2O_3 interface layer.

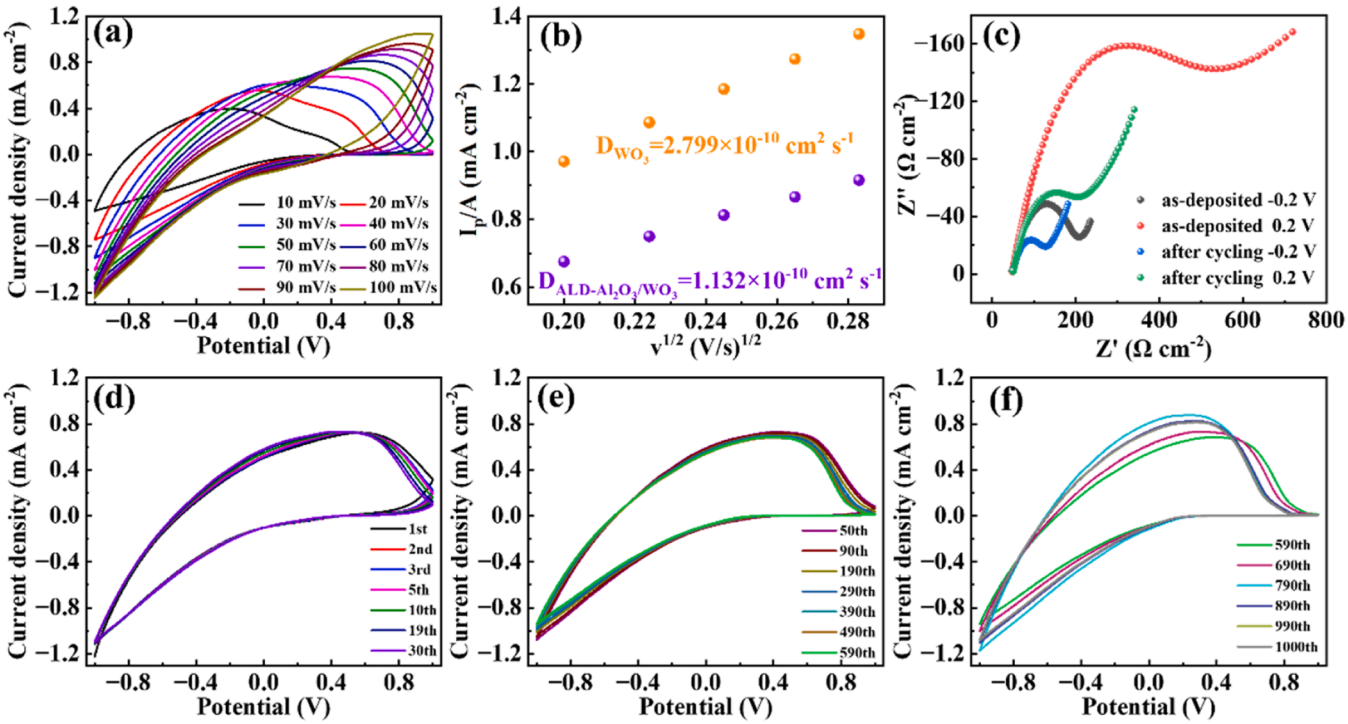

Fig. 5. (a) CV profiles at various scan rates for the WO_3 thin films with the ALD-Al_2O_3 interface layer. (b) Dependence of the peak current densities (I_p) versus the square root of scan rate ($v^{1/2}$). (c) Nyquist plot for the WO_3 thin films with the ALD-Al_2O_3 interface layer. (d–f) 1000 cycles of the WO_3 thin films with the ALD-Al_2O_3 interface layer.

diffusion barrier for Li ions, consequently decelerating kinetics and causing a decrease in rate capacity. The Nyquist plots in the frequency region ranging from 100 mHz to 100 kHz for the WO_3 thin film with the ALD-Al_2O_3 interface layer before/after 50 electrochemical cycles are provided in Fig. S11a and S11b. In the high-frequency region, the real axis (x-intercept) represents the resistance (R_s), and the diameter of the semicircle represents the charge transfer resistance (R_{ct}) in the electrolyte. It can be seen that the Rct of the WO_3 thin films with the ALD-Al_2O_3 layer is significantly reduced from 159.6 Ω cm^{-2} to 87.6 Ω cm^{-2} at −0.2 V, and from 853 Ω cm^{-2} to 187 Ω cm^{-2} at 0.2 V after 50 electrochemical cycles, as shown in Fig. 5c, indicating that formation of the stable and Li-ion permeable SEI on the WO_3 thin film with the ALD-Al_2O_3 interface layer after cycling (Scheme 1).

To further investigate the impact of ALD interface layer on the reduction/oxidation reaction of WO_3 thin film during cycling, 1000 CV tests are performed for the WO_3 thin film with the ALD-Al_2O_3 interface layer at a scan rate of 50 mV s^{-1} within the range of −1.0 to 1.0 V. Fig. 5d depicts the CV curves from the first to the 30th cycle, a higher current density value appears at 1.0 V in the first cycle. It can be seen that the oxidation peak of CV curve in the range of 0.4 to 0.8 V gradually

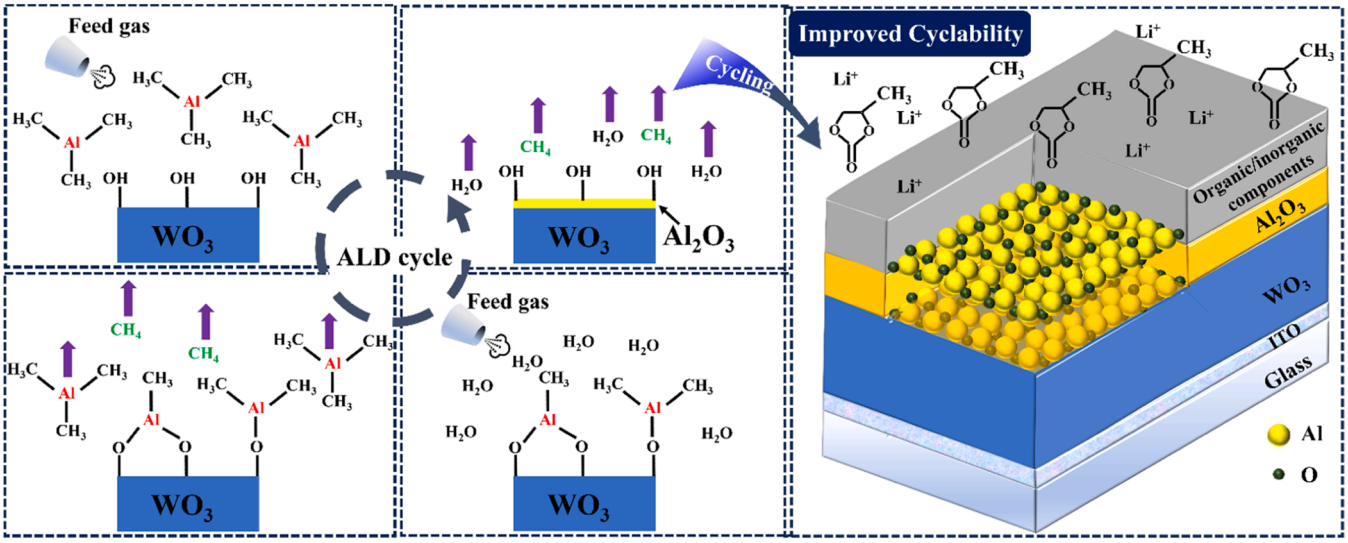

Scheme 1. The formation process of the SEI.

completed but with almost no change in its area and the reduction peak of CV curve remained unchanged with increasing cycle number, representing an increase in the rate of Li^+ de-intercalation, and SEI of the WO_3 thin film with the ALD-Al_2O_3 interface layer has formed preliminarily. As shown in Fig. 5e, the oxidation peak of the WO_3 thin film with the ALD-Al_2O_3 interface layer gradually shifted negatively, accompanying with the decrease in the peak current density as the number of CVs increases. Furthermore, with the increase of CV cycle number, the potential differences (ΔV) between the oxidation and reduction peaks became smaller. Generally, the electrode with the ALD-Al_2O_3 interface layer displays larger ΔV than the bare one, indicating a larger electrochemical polarization [41,42]. The Al_2O_3/Li-based electrolyte hybrid SEI layer remains stable and effective at this stage. Between the 590th and 1000th cycle, a more noticeable change is observed in Fig. 5f. The WO_3 thin film with the ALD-Al_2O_3 interface layer took 790 cycles to reach the maximum peak current density accompanying with a small decrease, and the oxidation peak continuously shifting negatively. These changes may be attributed to the gradual destruction of the SEI layer, resulting in direct contact between the WO_3 thin film and the electrolyte, the amount of Li^+ intercalation and de-intercalation on thin film increases. At the 1000th cycle, the oxidation peak position has moved to 0 to 0.4 V, the same as the WO_3 thin film without the ALD-Al_2O_3 interface layer (Fig. S11c).

4. Conclusion

In summary, we have demonstrated that the established *in situ* SEI protection is a feasible strategy to improve the cycling stability of WO_3 thin film. By depositing a 1-nm-thick Al_2O_3 interface layer on the WO_3 thin film using ALD prior to the initial cycling process, the formation of side-reaction products formation is constrained by the surrounding Al_2O_3 layer. This allows for quicker interface densification and *in situ* formation of organic/inorganic hybrid solid electrolyte interphase on the WO_3 thin film during electrochemical cycling. Thus, the WO_3 thin film with the ALD-Al_2O_3 interface layer maintains 94 % transmittance modulation retention after 1500 cycles. These findings provide unambiguous evidence for the effectiveness of the ALD-Al_2O_3 interface layer in protecting WO_3 and offer methodologies for further investigations into impact of this approach on other EC layer materials.

CRediT authorship contribution statement

Shichen Weng: Writing – original draft, Visualization, Validation, Software, Methodology, Investigation, Data curation. **Chengli Zhang:** Project administration, Funding acquisition. **Qiang Wang:** Visualization, Investigation, Data curation. **Guanglong Xu:** Visualization, Investigation, Data curation. **Jumei Zhou:** Methodology, Investigation, Funding acquisition. **Kunrun Song:** Data curation, Conceptualization. **A.A. Rogachev:** Validation. **M.A. Yarmolenko:** Validation. **Hongtao Cao:** Supervision, Resources, Project administration, Funding acquisition. **Hongliang Zhang:** Writing – review & editing, Supervision, Resources, Project administration, Methodology, Funding acquisition.

Declaration of competing interest

The authors declare that they have no known competing financial interests or personal relationships that could have appeared to influence the work reported in this paper.

Data availability

No data was used for the research described in the article.

Acknowledgements

This project is supported by the International Cooperation Project of Ningbo City (2023H003), National Natural Science Foundation of China (61974148) and Natural Science Foundation of Zhejiang Province (LY23F040003).

Supplementary materials

Supplementary material associated with this article can be found, in the online version, at doi:10.1016/j.surfin.2024.103992.

References

[1] A. Llordes, G. Garcia, J. Gazquez, D.J. Milliron, Tunable near-infrared and visible-light transmittance in nanocrystal-in-glass composites, Nature 500 (7462) (2013) 323–327, https://doi.org/10.1038/nature12398.
[2] J.B. Pan, R.Z. Zheng, Y. Wang, X.K. Ye, Z.Q. Wan, C.Y. Jia, X.L. Weng, J.L. Xie, L. J. Deng, A high-performance electrochromic device assembled with hexagonal WO_3 and NiO/PB composite nanosheet electrodes towards energy storage smart window, Sol. Energy Mater. Sol. Cells 207 (2020) 110337, https://doi.org/10.1016/j.solmat.2019.110337.
[3] H.L. Zhang, S. Liu, T. Xu, W.P. Xie, G.X. Chen, L.Y. Liang, J.H. Gao, H.T. Cao, Aluminum-ion-intercalation nickel oxide thin films for high-performance

electrochromic energy storage devices, J. Mater. Chem. C 9 (48) (2021) 17427–17436, https://doi.org/10.1039/d1tc04240h.
[4] W. Zhang, H.Z. Li, M. Al-Hussein, A.Y. Elezzabi, Electrochromic battery displays with energy retrieval functions using solution-processable colloidal vanadium oxide nanoparticles, Adv. Opt. Mater. 8 (2) (2020) 1901224, https://doi.org/10.1002/adom.201901224.
[5] R.R. Ren, S.Y. Liu, Y. Gao, P.Y. Lei, J.H. Wang, X.R. Tong, P. Zhang, Z.P. Wang, G. F. Cai, Tunable interaction between Zn^{2+} and superstructured $Nb_{18}W_{16}O_{93}$ bimetallic oxide for multistep tinted electrochromic device, ACS Energy Lett. 8 (5) (2023) 2300–2307, https://doi.org/10.1021/acsenergylett.3c00484.
[6] G.F. Cai, R. Zhu, S.Y. Liu, J.H. Wang, C.Y. Wei, K.J. Griffith, Y. Jia, P.S. Lee, Tunable intracrystal cavity in tungsten bronze-like bimetallic oxides for electrochromic energy storage, Adv. Energy Mater. 12 (5) (2022) 2103106, https://doi.org/10.1002/aenm.202103106.
[7] K. Wang, H.L. Zhang, W.P. Xie, G.X. Chen, R. Jiang, K. Tao, L.Y. Liang, J.H. Gao, H. T. Cao, Unraveling the role of water on the electrochromic and electrochemical properties of nickel oxide electrodes in electrochromic pseudocapacitors, J. Electrochem. Soc. 168 (11) (2021) 113502, https://doi.org/10.1149/1945-7111/ac3527.
[8] Z.H. Wang, X. Zhang, H.L. Zhang, F.F. Ge, Q. Wang, C.L. Zhang, G.L. Xu, J.H. Gao, A.A. Rogachev, H.T. Cao, Real-time mass change: an intrinsic indicator to dynamically probe the electrochemical degradation evolution in WO_3, Adv. Mater. Interfaces 9 (19) (2022) 2200340, https://doi.org/10.1002/admi.202200340.
[9] E.D. Rus, J.A. Dura, *In situ* neutron reflectometry study of a tungsten oxide/Li-ion interface, ACS Appl. Mater. Interfaces 15 (2) (2023) 2832–2842, https://doi.org/10.1021/acsami.2c16737.
[10] L.D. Xing, X.W. Zheng, M. Schroeder, J. Alvarado, A.V. Cresce, K. Xu, Q.S. Li, W. S. Li, Deciphering the ethylene carbonate-propylene carbonate mystery in Li-ion batteries, Acc. Chem. Res. 51 (2) (2018) 282–289, https://doi.org/10.1021/acs.accounts.7b00474.
[11] S. Liu, H.L. Zhang, X. Zhang, Q. Wang, C.L. Zhang, R. Jiang, J.H. Gao, L.Y. Liang, H. T. Cao, Understanding electrochemical intercalation of Al^{3+} cation into the WO_3 electrochromic electrode from solid electrolyte interphase and mass changes, ACS Appl. Energy Mater. 5 (2) (2022) 1833–1839, https://doi.org/10.1021/acsaem.1c03242.
[12] Q.J. Huang, G.B. Dong, Y. Xiao, X.G. Diao, Electrochemical studies of silicon nitride electron blocking layer for all-solid-state inorganic electrochromic device, Electrochim. Acta 252 (2017) 331–337, https://doi.org/10.1016/j.electacta.2017.08.177.
[13] K.R. Reyes-Gil, Z.D. Stephens, V. Stavila, D.B. Robinson, Composite WO_3/TiO_2 nanostructures for high electrochromic activity, ACS Appl. Mater. Interfaces 7 (4) (2015) 2202–2213, https://doi.org/10.1021/am5050696.
[14] Y.C. He, F. Zhang, Q.Q. Zhang, G.B. Dong, X.L. Zhong, X.G. Diao, High capacity and performance lithium based electrochromic device via amorphous tantalum oxide protective layer, Electrochim. Acta 280 (2018) 163–170, https://doi.org/10.1016/j.electacta.2018.05.123.
[15] K. Wang, D. Qiu, H.L. Zhang, G.X. Chen, W.P. Xie, K. Tao, S.H. Bao, L.Y. Liang, J. H. Gao, H.T. Cao, Boosting charge-transfer kinetics and cyclic stability of complementary WO_3-NiO electrochromic devices via SnO_x interfacial layer, J. Sci. Adv. Mater. Devices 6 (3) (2021) 494–500, https://doi.org/10.1016/j.jsamd.2021.06.001.
[16] P. Shen, H. Huang, A.C.C. Tseung, Improvements in the life of WO_3 electrochromic films, J. Mater. Chem. 2 (5) (1992) 497–499, https://doi.org/10.1039/jm9920200497.
[17] H.Y. Qiu, X.F. Du, J.W. Zhao, Y.T. Wang, J.W. Ju, Z. Chen, Z.L. Hu, D.P. Yan, X. H. Zhou, G.L. Cui, Zinc anode-compatible *in-situ* solid electrolyte interphase via cation solvation modulation, Nat. Commun. 10 (2019) 5374, https://doi.org/10.1038/s41467-019-13436-3.
[18] J. Wan, Y. Hao, Y. Shi, Y.X. Song, H.J. Yan, J. Zheng, R. Wen, L.J. Wan, Ultra-thin solid electrolyte interphase evolution and wrinkling processes in molybdenum disulfide-based lithium-ion batteries, Nat. Commun. 10 (2019) 3265, https://doi.org/10.1038/s41467-019-11197-7.
[19] C. Yan, R. Xu, Y. Xiao, J.F. Ding, L. Xu, B.Q. Li, J.Q. Huang, Toward critical electrode/electrolyte interfaces in rechargeable batteries, Adv. Funct. Mater. 30 (23) (2020) 1909887, https://doi.org/10.1002/adfm.201909887.
[20] A.L. Lipson, K. Puntambekar, D.J. Comstock, X.B. Meng, M.L. Geier, J.W. Elam, M. C. Hersam, Nanoscale investigation of solid electrolyte interphase inhibition on Li-ion battery MnO electrodes via atomic layer deposition of Al_2O_3, Chem. Mater. 26 (2) (2014) 935–940, https://doi.org/10.1021/cm402451h.
[21] Z. Zhao, G.S. Huang, Y. Kong, J.Z. Cui, A.A. Solovev, X.F. Li, Y.F. Mei, Atomic layer deposition for electrochemical energy: from design to industrialization, Electrochem. Energy Rev. 5 (SUPPL 1) (2022), https://doi.org/10.1007/s41918-022-00146-6.
[22] J. Liu, X.L. Sun, Elegant design of electrode and electrode/electrolyte interface in lithium-ion batteries by atomic layer deposition, Nanotechnology 26 (2) (2015), https://doi.org/10.1088/0957-4484/26/2/024001.
[23] H.C.M. Knoops, M.E. Donders, M.C.M. van de Sanden, P.H.L. Notten, W.M. M. Kessels, Atomic layer deposition for nanostructured Li-ion batteries, J. Vac. Sci. Technol. A 30 (1) (2012), https://doi.org/10.1116/1.3660699.
[24] K. Wang, H.L. Zhang, G.X. Chen, T. Tian, K. Tao, L.Y. Liang, J.H. Gao, H.T. Cao, Long-term-stable WO_3-PB complementary electrochromic devices, J. Alloys Compd. 861 (2021) 158534, https://doi.org/10.1016/j.jallcom.2020.158534.
[25] K. Lim, M. Hagel, K. Kuster, B. Fenk, J. Weis, U. Starke, J. Popovic, J. Maier, Chemical stability and functionality of Al_2O_3 artificial solid electrolyte interphases on alkali metals under open circuit voltage conditions, Appl. Phys. Lett. 122 (9) (2023) 093902, https://doi.org/10.1063/5.0123535.
[26] X.Y. Dai, A.J. Zhou, J. Xu, B. Yang, L.P. Wang, J.Z. Li, Superior electrochemical performance of $LiCoO_2$ electrodes enabled by conductive Al_2O_3-doped ZnO coating via magnetron sputtering, J. Power Sources 298 (2015) 114–122, https://doi.org/10.1016/j.jpowsour.2015.08.031.
[27] A.C. Kozen, C.F. Lin, A.J. Pearse, M.A. Schroeder, X.G. Han, L.B. Hu, S.B. Lee, G. W. Rubloff, M. Noked, Next-generation lithium metal anode engineering via atomic layer deposition, ACS Nano 9 (6) (2015) 5884–5892, https://doi.org/10.1021/acsnano.5b02166.
[28] T.H. Fleisch, G.J. Mains, An XPS study of the UV reduction and photochromism of MoO_3 and WO_3, J. Chem. Phys. 76 (2) (1982) 780–786, https://doi.org/10.1063/1.443047.
[29] X.R. Tong, J.H. Wang, P. Zhang, P.Y. Lei, Y. Gao, R.R. Ren, S.Y. Zhang, R. Zhu, G. F. Cai, Insight into the structure-activity relationship in electrochromism of WO_3 with rational internal cavities for broadband tunable smart windows, Chem. Eng. J. 470 (2023) 144130, https://doi.org/10.1016/j.cej.2023.144130.
[30] H.H. Liu, Y.M. Zhang, P.Y. Lei, J.F. Feng, S.S. Jia, J.J. Huang, C.Y. Hu, C.C. Bian, G. F. Cai, Selective electrochromic regulation for near-infrared and visible light via porous tungsten oxide films with core/shell architecture, ACS Appl. Mater. Interfaces 15 (19) (2023) 23412–23420, https://doi.org/10.1021/acsami.3c01742.
[31] C.C. Wang, W.L. Su, Ultrathin artificial solid electrolyte interface layer-coated biomass-derived hard carbon as an anode for sodium-ion batteries, ACS Appl. Energy Mater. 5 (1) (2022) 1052–1064, https://doi.org/10.1021/acsaem.1c03425.
[32] Z.H. Wang, G.X. Chen, H.L. Zhang, L.Y. Liang, J.H. Gao, H.T. Cao, *In situ* TEM investigation of hexagonal WO_3 irreversible transformation to Li_2WO_4, Scr. Mater. 203 (2021) 114090, https://doi.org/10.1016/j.scriptamat.2021.114090.
[33] K. Chandrasiri, C.C. Nguyen, Y.Z. Zhang, B.S. Parimalam, B.L. Lucht, Systematic investigation of alkali metal ions as additives for graphite anode in propylene carbonate based electrolytes, Electrochim. Acta 250 (2017) 285–291, https://doi.org/10.1016/j.electacta.2017.08.065.
[34] Q. Zhang, C. Zhou, M.H. Li, Y.M. Zhu, X.B. Wei, S.C. Shen, Z.W. Ji, G.F. Luo, Y. F. Cheng, X.M. Yang, Z.J. Wang, L.F. Zou, L. Zeng, J.H. Lin, L. Li, J.S. Francisco, M. Gu, Revealing structural insights of solid electrolyte interphase in high-concentrated non-flammable electrolyte for Li metal batteries by cryo-TEM, Small 19 (28) (2023) 2300849, https://doi.org/10.1002/smll.202300849.
[35] K.I. Chung, J.D. Lee, E.J. Kim, W.S. Kim, J.H. Cho, Y.K. Choi, Studies on the effects of coated Li_2CO_3 on lithium electrode, Microchem. J. 75 (2) (2003) 71–77, https://doi.org/10.1016/s0026-265x(03)00026-2.
[36] Q.Y. Zhang, J.L. Ma, L. Mei, J. Liu, Z.Y. Li, J. Li, Z.Y. Zeng, *In situ* TEM visualization of LiF nanosheet formation on the cathode-electrolyte interphase (CEI) in liquid-electrolyte lithium-ion batteries, Matter 5 (4) (2022) 1235–1250, https://doi.org/10.1016/j.matt.2022.01.015.
[37] D. Aurbach, Review of selected electrode-solution interactions which determine the performance of Li and Li ion batteries, J. Power Sources 89 (2) (2000) 206–218, https://doi.org/10.1016/s0378-7753(00)00431-6.
[38] J.G. Thevenin, R.H. Muller, Impedance of lithium electrodes in a propylene carbonate electrolyte, J. Electrochem. Soc. 134 (2) (1987) 273–280, https://doi.org/10.1149/1.2100445.
[39] S.L. Zhang, S. Cao, T.R. Zhang, J.Y. Lee, Plasmonic oxygen-deficient $TiO_{(2-x)}$ nanocrystals for dual-band electrochromic smart windows with efficient energy recycling, Adv. Mater. 32 (43) (2020) 2004686, https://doi.org/10.1002/adma.202004686.
[40] H. Yu, J.J. Guo, C. Wang, J.Y. Zhang, J. Liu, X.L. Zhong, G.B. Dong, X.G. Diao, High performance in electrochromic amorphous WO_x film with long-term stability and tunable switching times via Al/Li-ions intercalation/deintercalation, Electrochim. Acta 318 (2019) 644–650, https://doi.org/10.1016/j.electacta.2019.06.129.
[41] H.T.H. Chan, E. Katelhon, R.G. Compton, Voltammetry using multiple cycles: porous electrodes, J. Electroanal. Chem. 799 (2017) 126–133, https://doi.org/10.1016/j.jelechem.2017.05.043.
[42] C.Q. Fu, J.H. Qu, Z.H. Dan, F.X. Qin, Y. Zhang, N. Hara, H. Chang, L. Zhou, Enhanced redox properties of amorphous $Fe_{63.3-83.3}Co_{0-20}Si_4B_8P_4Cu_{0.7}$ alloys via long-term CV cycling, J. Alloys Compd. 751 (2018) 349–358, https://doi.org/10.1016/j.jallcom.2018.04.119.